Chapter 2

The Emulsion Technique and Data Characteristics

In this chapter, the experimental aspects of the present investigation have been outlined. Salient features of the nuclear emulsion technique have been described in general terms. The optical microscopy, that is so intimately associated with the data acquisition process, has also been briefly discussed. The limitations of this age old technique, as well as its advantages in the perspective of the methods of data analysis adopted subsequently, have been critically scrutinized. A data sample of ^{32}S-Ag/Br interactions at an incident momentum of 200A GeV/c, has been analyzed in the present investigation. Some of the general characteristics of this data sample, that are pertinent to our methods of analysis, have been incorporated for better understanding the issues discussed in subsequent chapters. A data sample generated by the Lund Monte Carlo Code FRITIOF has been used for comparison with the experiment. Gross features of the generated data sample have also been included.

2.1 Nuclear Emulsion Technique

The first use of photographic emulsion to record charged particle tracks was made in 1911, when alpha particles were found to affect silver bromide grains along their paths in such a way as to be later developed to metallic silver [1]. However, its only around the 1940s that the nuclear emulsion technique matured as an effective and successful tool for research in cosmic ray, nuclear and particle physics. This became possible due to the efforts of firms like the Ilford Ltd. (London), the Kodak Ltd. (New York), and to a great extent due to the contribution of the emulsion research group in the University of Bristol (UK). The usefulness of this technique can be understood from its rich history of being a key detector in discovering several new particles like the charged π-mesons, the charged K-mesons, the Σ^+ and the $\bar{\Lambda}$ baryons etc. In spite of a stiff competition offered by its more prestigious and much costlier large electronic counterparts, even in the recent past the emulsion experiments have contributed significantly in studying different phenomena in high-energy hA and AB interactions. Besides its use in high-energy research, emulsions are currently also being used in medical, biological and geophysical research, in metallurgy and in studying chemically active surfaces. Throughout the world there are several firms and/or institutes who manufacture nuclear research emulsions e.g, the Ilford Ltd. (London), the Eastman Kodak Company (Rochestar), the NIKFI Institute (Moscow), the Fuji Films Ltd. (Tokyo) etc. The Ilford G5 type of nuclear emulsion has been used in the present investigation. In the following discussion therefore, if otherwise not mentioned, we shall refer to emulsion characteristics and parameters pertaining only to this particular type. Excellent reviews and texts [2–4] are available on the details of nuclear emulsion technique. However, in the following sections we have tried to summarize its essential features.

2.1.1 Nuclear Emulsion

Any photographic emulsion is basically a dispersion of silver halide crystals within a gelatin matrix. Nuclear emulsions used for recording charged particle tracks consist of silver halide micro-crystals embedded into about equal parts in volume, a matrix material comprising mainly of gelatin and water with a small amount of glycerol and a few other substances. Silver halide, usually in the form of silver bromide crystals, also contains a

small amount of iodine in the crystal lattice. Ionizing (electrically charged) particles, while passing through such emulsions leave behind them silver halide crystals so altered, that upon proper chemical treatment, they appear as a trail of black colloidal grains of metallic silver along the trajectories of the particles. However, compared to the general purpose photographic emulsions the nuclear emulsions have several distinguishing features. In nuclear emulsion plates the photosensitive silver halide material (mostly AgBr) has three to four times more concentration than that in the conventional photographic plates. The nuclear emulsion plates are also made much thicker - a few hundreds to several hundreds of microns as compared to only several microns in case of ordinary photographic plates. The AgBr grains in nuclear emulsion are well separated and are much smaller in size (less than a micron in diameter). Whereas in ordinary photographic plates, the grains are interlocked and the grain diameter can be as large as several microns. Though the silver halide crystals in nuclear emulsion are very uniform in size, it is observed that in any particular sample the grains are actually distributed about a mean value with a small but certain variance in diameter. For Ilford G.5 emulsion the mean grain diameter is $\approx 0.3\mu$m. However, the mean crystal grain diameters are usually different for different types of emulsions. It is observed that the contrast of nuclear emulsion may be improved if the grains are uniform in size, whereas, the sensitivity goes up with increasing grain size. In nuclear emulsion there are very few crystals that can be developed without exposure to a charged particle.

As mentioned above, thickness of emulsion pellicles (films without any glass plate backing) ranges from $\sim 10^2\mu$m to a few millimeters, whereas the length (breadth) usually is a few to several inches. In the present investigation the dimensions of Ilford G5 emulsion pellicles were $18 \times 7.5 \times 0.06$ cm^3. The pellciles are mounted on 1.3 mm thick glass plates and their extremely sensitive top surfaces are coated to avoid abrasion marks to be formed. Gelatin is a hygroscopic material and emulsion plates can absorb water from atmosphere. Their volume change with relative humidity shows a hysteresis effect. At around 58% of relative humidity, the volume per unit mass of emulsion during the absorption is found to be equal to that during the desorption process. As far as the composition of emulsion is concerned, it is therefore necessary to refer to the relative humidity value. Each gram of Ilford nuclear emulsion contains 0.83 gm of silver halide and 0.162 gm of gelatine at

58% relative humidity; corresponding volume ratio is about 45 : 55. The percentage of moisture contents by weight in Ilford nuclear emulsions at 20^0C at various relative humidities are given below [2] in Table 2.1.

Table 2.1. Moisture content of Ilford emulsion at different relative humidities

Relative humidity	0	30	50	60	70	85
Moisture content	1.41	2.06	2.65	2.95	3.7	5.17

The accepted value of the density of silver halide crystal is $\approx$ 6.473 gm/cc. The density of supplied emulsion is 1.29 gm/cc at 58% relative humidity, which after drying may rise to 3.83 gm/cc in equilibrium with air at 20^0C at 58% relative humidity. In Table 2.2 the chemical composition of Ilford G5 type of emulsion is given [4].

Table 2.2 Composition of standard emulsion

Element	Atomic No. (Z)	Atomic weight (A)	Concentration at 58% R.H.	No. of atoms per cc $\times 10^{20}$	Moles per cc $\times 10^{-3}$
Ag	47	107.88	1.817	101.01	16.764
Br	35	79.916	1.338	100.41	16.673
I	53	129.93	0.012	0.565	0.094
C	6	12.0	0.277	138.30	22.698
N	7	14.008	0.0534	31.68	5.147
S	16	32.06	0.249	1.353	0.216
H	1	1.008	0.074	321.56	53.571
O	8	16.0	0.007	94.97	16.050

The total number of atoms available in emulsion per cc is 7.898×10^{22}, whereas, the total number of electrons available is 1.0446×10^{24} per cc. Taking the nuclear radius parameter $r_0 = 1.2\ fm$, the geometrical mean free path of all elements in nuclear emulsion will come out to be $\approx$ 37 cm. However, as we shall see later this geometrical mean free path is quite different from the interaction mean free path.

2.1.2 Latent Image Formation

The mechanism of developable (usually called 'latent') image formation in nuclear emulsion is essentially the same as that in the ordinary light sensitive photographic plates. But there is a significant difference between the two. In the former case this takes place through ionization of atoms present in the emulsion by electrostatic interaction with the passing charged particles. Whereas, in the latter case this occurs due to emission of photoelectrons by the incident light. The first comprehensive theory of the photolytic process underlying the latent image formation was provided by Gurney and Mott [5]. According to their principle both ionic and electronic conduction contribute during the process of latent image formation. They proposed that, as the incident particle passes through emulsion, photons are absorbed in the silver halide and some electrons are raised to the conduction band. These electrons are allowed to migrate freely until they encounter local minima of potential energy (called sensitivity specks), where they can be trapped. Such local minima are provided by colloidal silver and/or silver sulphide usually located on the crystal surface. The sensitivity specks are now negatively charged and are capable to attract interstitial silver ions (Ag^+) present within the crystal as Frenkel defects, which are free to move through the crystal lattice. The Ag^+ ions are neutralized by capturing the extra electrons and silver specks of sufficiently large size can grow as a stable development (latent image) center. At least three silver atoms adsorbed at the AgBr crystal surface are required to achieve stability. Latent image formation in nuclear emulsion is an inefficient process, particularly for fast moving charged particles. The migration of silver ions through the crystal is considerably slower than that of the electrons. Thus the sensitivity specks acquire negative charges more rapidly than their rate of getting neutralized by Ag^+ ions. Further electron conduction to a particular sensitivity speck is therefore, slowed down. The electrons being raised to conduction band by the moving particle would try to find other points in the crystal, thereby prohibiting any particular speck to grow sufficiently in size as a latent image. The Gurney-Mott theory was later modified by Mitchell and collaborators [6], where conduction of positive holes as well as recombination of holes and electrons were taken into account. However, the details of the theory of latent image formation is not one of the major objectives of the present discussion, and we have preferred to concentrate more on other aspects of the technique.

2.1.3 Emulsion Processing

Once the emulsion pellicles are irradiated by ionizing charged particles, they should be so processed as to be made suitable for scanning and measurement under optical microscopes. This requires the pellciles to undergo through several subprocesses like presoaking, development, stopping, fixing, washing, mounting on glass plates and drying. However, processing emulsion pellicles that are already mounted on glass plates is also very common. Through photographic development the latent images contained in an emulsion are made visible by reduction of silver ions in the silver halide crystals to metallic silver. A developer is usually chosen that reduces the crystals containing a latent image center completely and leaves those not containing a center unchanged. Before development the pellicles are often presoaked in distilled water to facilitate the developer to rapidly diffuse into the emulsion without affecting the actual development. The development time should be sufficient for the crystals with a latent image center to be reduced completely, but not so long that the unexposed crystals are developed. In practice, a certain number of crystals will be developed even though they do not contain a latent image center. These grains, when developed, constitute what is known as fog or background. While developing thick emulsion layers ($\sim$ several hundred microns), care should be taken regarding uniform development with minimum distortion. Techniques like 'temperature development' [7] and 'two bath development' [8] are found useful for uniform development. In the first technique the pellicles may be vertically immersed into the developer at sufficiently low temperature to inhibit its action, and to allow the developer to permeate into the entire bulk of each pellicle from both of its flat (length-breadth) sides. The developer is then slowly warmed and its action starts. In the second technique two developer solutions are employed in two different baths. The first one contains developing agents without any alkali, and the second one containing the same with excess alkali with a high pH environment. Immersing into the first bath will only permit the developing agents to diffuse into the emulsion layers, while in the second bath the actual development takes place. Developer formulations of two reagents from the Ilford Ltd. meant for Ilford G5 emulsions are given in Table 2.3 [9].

After completion of the development stage the developer action should be arrested immediately. For thick emulsions this is done by putting the pellicles into a stop bath that can

reduce their pH value, in conjunction with rapid cooling. An environment of dilute acetic acid ($\sim$ 1%) and a temperature $\sim 5^0$C is suitable for the purpose. Like development, stop bath time also varies with the thickness. Because of high concentration of AgBr in emulsions, and its partial solubility in the developer, a thin film of silver is formed on the surface of the pellicles during development. This surface deposit should be completely removed. This may be done in the stop bath itself with the help of a chamois leather or by finger tips. As the emulsion is in wet condition extreme care should be taken to prevent distortion.

Table 2.3 Developer Formulation

Developer type	Chemical component	Amount
ID-19	Metol	2.2 gm
	Anhydrous Sodium Sulphite	72 gm
	Hydroquinone	8.8 gm
	Anhydrous Sodium Carbonate	48 gm
	Potassium Bromide	4 gm
	Water to make	1 liter
Brussels Amidol	Anhydrous Sodium Sulphite	18 gm
	Potassium Bromide	0.8 gm
	Amidol	4.5 gm
	Boric Acid	35 gm
	Water to make	1 liter

The emulsion should then be fixed. The purpose of fixation is to remove all the residual silver halide, leaving the metallic silver to form the image. If any amount of silver halide is left in the emulsion, it would slowly break into ions and the plate will go brown degrading the quality of the image. The fixing agents most widely used are sodium or ammonium thiosulphate, which form thiosulphate complexes with the silver halide. Silver thiosulphate is soluble in water and so may be removed from the emulsion by washing. It is important to use a fixer that has not been exhausted while processing nuclear emulsions; otherwise some silver halide will remain in the emulsion. To ensure that the entire

silver halide is removed, a fixing time which is twice the time it takes for the emulsion to clear should be allowed. After fixation, the emulsion must be washed very thoroughly in tap water with a final rinse in distilled water to remove all the silver thiosulphate complexes in the emulsion. After washing is completed, the pellicles are mounted on glass plates slightly larger than the size of the pellicles and kept inside a refrigerator until they are set. The glass plates should have grid lines and grid numbers printed on them, so that an event once found out, can easily be relocated later. The glass plates should also have a gelatin coating on them. Drying of emulsion plates is then conducted at around 20^0C. A summary of the entire processing procedure for typical 600μm thick emulsion is summarized in the following Table [2].

Table 2.4 Processing of 600μm thick emulsion

Procedure	Temperature	Time
Presoaking in distilled water	ambient $\rightarrow$ 5^0C	100 min
Developer penetration (Brussels Amidol)	5^0C	100 min
Dry development	23^0C	20 min
Dry cooling	23^0C $\rightarrow$ 8^0C	5 min
Acid stop bath (1% acetic acid)	5^0C	100 min
Removal of surface deposit		
Fixation		
Clearing	5^0C	18 hrs
Dilution	5^0C	24 hrs
Washing	5^0C	24 hrs
Plasticizing solution (10% Ansco Flexiglass)	5^0C	30 min
Drying (relative humidity (100% $\rightarrow$ 50%)	5^0C	7 days

As gelatin and glycerin are both hygroscopic, the actual thickness and the refractive index of the processed and unprocessed emulsion depends on the surrounding humidity. During

the process of washing, developing and fixing there is a shrinkage in the vertical direction since the other two directions are fixed. Therefore, one has to introduce a shrinkage factor S and multiply the vertical measures to obtain the correct results for any quantitative measurement of grain density, range and angles in emulsion. Generally the shrinkage factor is supplied by the manufacturer of the emulsion plates. The shrinkage factor is defined as $S = T/t$, where T = the thickness of the emulsion layer at the time of exposure and t = that at the time of scanning.

2.1.4 Track Structure

Grain Density: The grain density dn/dx of a track is measured by the number of developed silver grains per unit path length. If the grains are discrete and the upper limit of the grain density is 50 grains per 100μm and the lower limit of the grain density is 20 grains per 100μm for a relatively low background plate (e.g., less than 4 grains per μm^2) the measurement of dn/dx is not too difficult one. But in actual case there are many blobs of individual grains which can not be resolved. For this purpose a grain count value (n) is assigned to unresolvable grain clumps. Fowler and Perkins considered that $n = 2.4l$, where l is the length of the clump in microns, when the average developed grain diameter is about $0.3 - 0.4\mu$m. For a particle of mass m, charge ze, and is moving with a velocity $v\,(= \beta\, c)$ that is large compared to the velocity of the K-shell electrons of the stopping material, the average restricted energy loss per unit distance is given by [10],

$$-\frac{dE}{dx} = \frac{4\pi\, z^2\, e^4\, N\, Z}{m\, v^2}\left[\ln\left(\frac{2m\, v^2}{I}\right) - \ln(1-\beta^2) - \beta^2\right], \tag{2.1}$$

where N is the number of atoms per cm^3 of the stopping material (in this case emulsion), Z and I are, respectively, the mean atomic number and ionization potential of the stopping material. It is assumed that there exists a direct proportionality between dE/dx of the particles at various points on their trajectories and the corresponding dn/dx. However, for high dE/dx values this proportionality can no longer remain valid. This is due to the inability of the sensitivity specks of the halide grains to acquire electrons produced in their vicinity by the passage of the charged particle at a sufficiently rapid rate to prevent the formation of a space charge with high electron densities, that ultimately results in an inefficiency of the electron utilization. For specific energy loss below a certain value, the

efficiency of electron utilization in terms of the proportion of electrons contributing to the latent image formation relative to the number initially produced is nearly constant, and this leads to the direct proportionality between dE/dx and dn/dx. For densities above 200 grains per 100μm grain saturation occurs, and it is impossible to evaluate dn/dx for such tracks on the basis of grain counts since the proportionality between n and l ceases to hold for such continuous grain distributions. For strongly ionized electrolytes, the potential of an ion cloud surrounding an isolated ion may be taken as $\propto \sqrt{N}$. Since N is proportional to dE/dx, an expression for dn/dx could be obtained in the form [11],

$$dn/dx = c\,\left[1 - \exp\left\{-b\,z\,(dE/dx)^{\frac{1}{2}} - a^{\frac{1}{2}}\right\}\right]. \tag{2.2}$$

Here 'b' and 'c' are constants that can be experimentally determined for the particular type of emulsion and developing material used, and 'a' is the minimum specific energy loss required to ensure developability of the grains.

Thus one can see that in order to estimate the specific energy loss dE/dx and hence the velocity of the moving charged particle, grain density is a useful parameter. Grain density is mainly determined by counting the number of developed grains within a measured length of the track. It is obvious that the error in measurement is less in case of low grain density. In case of high grain density the error automatically becomes large because the microscope cannot resolve the adjacent and overlapping grains. Sometimes instead of grain density, the blob density (B) is measured. A blob is the resolvable spot in which more than one grains may be present. The estimation of the number of blobs is equivalent to measuring the number of gaps between two blobs. O'Ceallaigh observed that the frequency distribution of the gap length has an exponentially decaying nature [12]. According to Fowler and Perkins [13] the number density of gaps (H) exceeding a value l is given by,

$$H(l) = B\,\exp\left(-g.\,l\right), \tag{2.3}$$

where the slope parameter g is a measure of the grain density, but cannot be set exactly equal to the true grain density dn/dx. Fowler and Perkins gave another relation as,

$$B = g\exp\left(-g.\alpha'\right), \tag{2.4}$$

where α' is a parameter determined by the average developed grain size. From Eq. 2.3 and 2.4 one can determine g as a useful ionizing parameter.

Lacunarity and Opacity: The lacunarity (L) of a track is defined as the fraction of the track made up of gaps, and it can be expressed as,

$$L = \int_0^\infty -l \left(\frac{dH}{dl}\right) dl \; = \; \exp(-g.\alpha').$$

Thus one can see that, $g = B/L$, and $\alpha' = -(L/B) \ln L$. For particles with low z and high velocity ($\beta \approx 1$), the restricted energy loss is small, and a simple proportionality like $dE/dx \propto dn/dx$ holds. Assuming $g \approx (dn/dx)$, one may therefore, write

$$z^2 \propto -\ln L. \tag{2.5}$$

One should keep in mind that for a given emulsion α' is constant, and for highly energetic particles variation in β with energy is also not significant. On the other hand the opacity (O) is defined as the fraction of a track made out of blobs, and it is related to lacunarity by the simple relation $O = 1 - L$. Thus the charge of a particle moving at relativistic speed can be determined by measuring its lacunarity or opacity [14]. A high degree of accuracy for such a measurement can be achieved because,

$$\delta z \propto \frac{1}{z} \frac{\delta L}{L},$$

where the error in lacunarity measurement,

$$\delta L = \frac{\sigma_L}{\sqrt{N_c}}$$

is seen to scale with $N_c^{-\frac{1}{2}}$, where N_c is the number of cells of equal length (say S) over which the measurement of L has been made, and one can arbitrarily increase the value of N_c. Here $\sigma_L = \sqrt{< L^2 > - < L >^2}$ is the variance in L.

Delta rays in Emulsion: Even for a particle moving with relativistic speed ($\beta \approx 1$), the grain density is very high if $z \geq 4$, and the track appears almost as a continuous black filament of silver. For such particles the rate of energy loss may be so large that, secondary electrons are produced with sufficient kinetic energies, and some of these electrons may have observable tracks within emulsion. Such electron tracks are known as the delta rays. The number of delta rays (n_δ) is a function of dE/dx, and the method of delta ray counting can therefore be utilized to determine the charge of a particle, where lacunarity measurement is not possible. The number of such delta rays with energies between W

and $W + dW$ had been calculated as [15],

$$dn_\delta = \frac{2\pi N z^2 e^4}{m_e v^2} \frac{dW}{W} \left[1 - \beta^2 \frac{W}{W_{max}}\right]. \tag{2.6}$$

Here m_e is the electron mass, and

$$W_{max} = \frac{2\, m_e\, c^2\, \beta^2\, \gamma^2}{1 + 2\left(\frac{m_e}{m}\right)\gamma + \left(\frac{m_e}{m}\right)^2} \tag{2.7}$$

is the upper energy limit that the electron may have received, and $\gamma \left[= \sqrt{1-\beta^2}\right]$ is the Lorentz factor associated with the moving particle. Whereas, W_{max} depends upon the sensitivity of the emulsion, the lower limit of W that defines a recognizable delta ray in emulsion, depends upon the range energy relation for low velocity electrons, the grain size, the scattering of these electrons, the sensitivity of the emulsion, and upon the criterion to distinguish the delta rays from random background grains. If a grain/blob configuration has to be counted as delta rays, the minimum acceptable track length has conventionally been chosen as $\approx 1.6\mu$m measured from the axis of the track of the moving particle. There are other conventions as well e.g., a minimum of four grains in a row. Both conventions give the lower limit of delta ray energy near 10 keV. Integrating dn_δ over dW, one finds that,

$$n_\delta \propto \frac{z^2}{\beta^2}. \tag{2.8}$$

For particles moving with relativistic speed $\beta \approx 1$, and hence the simple proportionality $n_\delta \propto z^2$ can be utilized to determine the charge of such a particle.

Range of a particle: Charged particles suffer collision with the atoms present in the medium through which it traverses, and looses energy as they ionize these atoms. The tracks terminate when the energy of the charged particles become less than the ionization potential of the atoms in the medium. The true range of an ionizing particle can be defined as the distance traveled by the particle with a given velocity v_0, before it stops within the emulsion. The measurable length of a track, sometimes also called the residual range (R), is the distance along its trajectory from the origin to the last developed silver grain on the track. This gives a measurement of the true range of the particle within a narrow limit. For low energy protons (kinetic energy ¡¡ rest energy) a range-energy relationship like, $R_p = K\, E_p^n$, has been theoretically obtained and also experimentally verified. Note that R is measured in microns, and E the kinetic energy in MeV. From

the knowledge about specific energy loss (dE/dx) and initial energy (E_0), the range of a particle can be determined as,

$$R(E_0) = \int_0^{E_0} \frac{dE}{dE/dx}.$$

Combining this relation with the expression for dE/dx (Eq. 2.1) one gets,

$$R(E_0) = \left(m/z^2\right) f(v_0).$$

In the nonrelativistic limit $(E_0 < mc^2)$ the energy ratio of two particles with same v_0, is same as their mass ratios. In this region for any particle a range-energy relation similar to that of the proton, has been experimentally observed to hold true for any particle. It is therefore, possible to determine the range-energy relation for an arbitrary particle as [16],

$$E = K \left(\frac{m}{m_p}\right)^{(1-n)} z^{2n} R^n, \tag{2.9}$$

where m_p is the proton rest mass, and $K = 0.262$ and $n = 0.575$ are two experimentally obtained parameters. Due to different types of uncertainties and fluctuations, ranges of even monoenergetic particles exhibit straggling. The straggling parameter may be defined as,

$$\Gamma_R = \left(\frac{\pi}{2}\right) \left[\frac{\sum_i^N \left(R_i - \bar{R}\right)^2}{N}\right]^{\frac{1}{2}}$$

or, as the full width at half maximum of the differential distribution curve of the ranges, that is related to Γ_R as, $\Delta R = 0.94\,\Gamma_R$.

Track Width: For high ionization (say $z > 10$), the linear track structure contains little information in terms of grain (or blob) density, and n_δ becomes too large to be counted. Under such circumstances, the track width has been found to be a useful parameter to identify the nature of the particle [4]. The track width depends on various factors such as, the type of emulsion, the type of developer used, the particle variables (charge, mass, velocity) etc.. It's also not an easy task to accurately determine the track width and correlate the data with particle identity. Accurate eyepiece micrometers should be used to measure the track width. The track image under high magnification ($\sim$ several thousand times) may be projected, and the area of a particular segment may be determined with a planimeter. The photoelectric opacity may also be used to digitally measure the track width. Experimental data show that the track width increases linearly with particle

charge for $z > 10$. As a track caused by a heavy nucleus/ion reaches towards its end, a thinning down (tapering) of the track is observed due to electron capture, which reduces the effective charge of the nucleus/ion. The length of this tapered portion (L_t) of the track may also be used to find out the atomic number of the particle [17]. An empirical relation like $L_t = C\, z^{\nu}$: $(\nu \approx 1)$ has been obtained in this connection.

2.2 The Microscopy

A good compound microscope is the main equipment for analyzing the behavior of tracks in emulsion. Emulsion microscopy is significantly different from other microscopy techniques such as those used in biological or material sciences [3, 4]. The horizontal area that has to be scanned is always much larger in size and there is always a greater emphasis on the vertical dimension. Searching for events within a three dimensional space requires fine focus mechanism. The length (or displacement) measuring devices attached to the stage supporting the subject (emulsion) must also posses a high degree of accuracy in all three (two horizontal and one vertical) directions. The stage movement must be very smooth and should be as much noise free as is possible. The most important component of a compound microscope is its objective(s). For minimum spherical aberration, achromatic objective lenses are made using combinations of convex and concave lenses with different refractive indexes and dispersions. The quality of measurement can be improved by creating a homogeneous optical medium. This is achieved by filling up the interstitial space between the objective and the emulsion with a material (often cedar wood oil), that has approximately the same refractive index (≈ 1.52) as that of the glass and gelatin. The resolution of the microscope depends of its numerical aperture. The numerical aperture ($N.A.$) is given by,

$$N.A. \;=\; \mu \,\sin\alpha,$$

where μ is the refractive index and α is the semivertex angle of the light ray cone that a point object extends toward the objective lens aperture. The minimum separation (d) between two adjacent points (not self luminous) that can just be separated is about

$$d \;\approx\; \frac{\lambda}{2\,\mu\,\sin\alpha}$$

where λ is the wave length of the light used in air. For dry lenses the $N.A. < 1$, whereas that for wet oil immersion type of objectives can be as high as 1.6. The depth of focus given by,

$$\Delta = \frac{\lambda}{4\,\mu\,\sin^2\left(\frac{\alpha}{2}\right)}$$

is a vertical length along the axis of the objective over which the sharpness of the visual image remains unchanged. Δ can vary from several microns for dry lenses ($N.A. < 0.25$ or so), to a fraction of a micron for wet lenses ($N.A. > 1$). For rapid scanning the dry lenses with low magnification are useful for rapid scanning, and the wet lenses are more suitable for critically scrutinizing an event and for accurate measurements. The working distance between an oil immersion objective must be of the order of a few mm for thick emulsion plates. Objectives should be parfocally mounted on a turret so that the axis of each lens is aligned to the same position, and each lens focuses at the same depth. A tube length of $160 - 170$ mm gives the best image produced by the objective lenses. A two element eyepiece (either Huygen or Ramsden type) consisting of one field lens and one eye lens, may be used to magnify the real image produced by the objective. Now-a-days more complex apochromatic structures are used, that can remove the secondary spectrum from the image and can also eliminate the chromatic effects of spherical aberration. Wide field viewing is an essential feature of nuclear track microscopy. This is limited by the diameter of the binocular eye tube. Binocular tubes with large diameter coupled with wide field ocular lenses are recommended for the purpose. Measurement within the field of view can be made with the help of a micrometer scale (called the graticule), which for a Ramsden type of eyepiece should be placed in front of the field lens. The graticule along with a goniometer can be employed to angle measurements. But such an arrangement is suitable only in those cases, where the tracks are angularly well separated from each other. In ^{32}S-Ag/Br interactions at 200A GeV/c one often encounters very dense jets of produced particles. For such cases one has to move the sample over quite a few number of fields of view, and measure the corresponding displacements using measuring devices attached with the mechanical stage. In all three directions the noise level associated with the stage motion should be as small as a fraction of a micron over a few centimeter of displacement. A microscope that can be used for nuclear track scanning probably desires the following features.

(a) 100× oil immersion objective with a working distance at least 500μ, 40× oil, 20× dry and a 10× dry objectives.

(b) A turret mount, co-centered well enough so that the middle of the field of any of the objectives will be found in the field of the 100× objective with a tolerance not more than one thousandth of an inch. Each lens length should be so adjusted that the lenses are parfocal on rotating turret.

(c) A binocular body with separate focus control of one ocular and sufficient range of interocular distance. Parallel eye tubes are preferred.

(d) Standard wide field oculars (10×, 15×).

(e) A goniometer for the dominant eye ocular with a graticule of good quality.

(f) A condensing lens with an numerical aperture of at least 1.25 and possibly another long working distance with an numerical aperture of about 1.00.

(g) A mechanical stage of sufficient area with sufficiently long stage motion along either of the perpendicular directions in the horizontal plane for the largest plate to be scanned.

2.2.1 Counting and statistics

In an emulsion experiment counting is as important as measurement. The emulsion provides discrimination between various sorts of events as well as different types of tracks emanating from an event. Events and tracks belonging to different categories should be properly counted. The ionization of a track may be measured by counting the number of grains or blobs over a particular length of the track (say 100 μm). Delta rays over a similar length interval may be counted to help identify the charge of the particle producing a track. Energy spectra are determined by counting the number of tracks within particular range intervals. Angular distributions are determined by counting the number of tracks in prescribed angular intervals. Prong numbers are counted to measure the excitation energy of an event. Therefore, in order to find out the reliability of the collected data, a practical knowledge of counting statistics is required. Three standard statistical distribution functions are often used for this purpose [4]. The Poisson distribution is given by,

$$P\left(n, \langle n \rangle\right) = \frac{\langle n \rangle^n \; e^{-\langle n \rangle}}{n!} \tag{2.10}$$

where $P(n)$ is the probability of occurrence of exactly n counts in a fairly large number of trials. The Poisson distribution is often used to describe the distribution of a random uncorrelated variable. The variance $\sigma^2 =< n^2 > - < n >^2$ of a Poisson distributed quantity is equal to the average $< n >$. If in a trial the probability of occurrence is finite (say q), the probability for a count n in m number of trials is described by the Binomial distribution,

$$P(n, m, < n >) = \frac{m!}{n!(m-n)!}\left(1 - \frac{< n >}{m}\right)^{m-n}\left(\frac{< n >}{m}\right)^{n}. \tag{2.11}$$

The Binomial distribution under special conditions reduces to a Poisson distribution. For Binomial distribution the average count is $< n >= mq$, and the variance is $\sigma^2 =< n >$ $(1- < n > /m)$. For large $< n >$ and m the Binomial expression converges to the Normal or Gaussian distribution,

$$P\left(n, \langle n \rangle, \sigma\right) = \frac{\exp[-\left(n - \langle n \rangle\right)^2 / 2\sigma^2]}{\sigma\sqrt{2\pi}}. \tag{2.12}$$

The mean absolute deviation (μ) of n from $\langle n \rangle$ is given by $\mu = \sigma\sqrt{2/\pi} = 0.7979\sigma$. In counting measurement this as convenient a measure of the statistical spread of the data as the standard deviation (σ). The probable error (ϵ) is estimated from $\epsilon = 0.6745\sigma$. Besides counting it is also often necessary to fit a set of data with a particular trend line. The Pearson's product moment correlation co-efficient (r), also known as the co-efficient of determination, is an indicator of how closely the estimated values corresponding to a particular trend line match with a set of data [18]. For a set of known pairs of variables $(x_i, y_i) : \ i = 1, \cdots, N$, the co-efficient is defined as,

$$r = \frac{N(\sum x_i\, y_i) - (\sum x_i)(\sum y_i)}{\sqrt{[N\sum x_i^2 - (\sum x_i^2)]\,[N\sum y_i^2 - (\sum y_i^2)]}}, \tag{2.13}$$

where N is the total number of data points. r is a dimensionless index and can range from $+1.0$ (a perfect positive linear correlation) to -1.0 (a perfect negative linear correlation). On the other hand $r = 0$ would indicate absence of any such correlation. The r^2 value may be interpreted as the proportion of variance in the dependent variable y_i that can be attributed to the variance in the independent variable x_i. For a straight line fit to the data $r^2 = 1.0$ means no discrepancy between observed and expected values. Another measure of discrepancy between observed and expected values (say frequency) is given by

the χ^2 statistic defined as,

$$\chi^2 = \sum_{i=1}^{N} \frac{(exp_i - obs_i)^2}{exp_i} \tag{2.14}$$

where exp_i (obs_i) denotes the expected (observed) frequencies, and $N = \sum obs_i = \sum exp_i$ denotes the total frequency. In case of dependent variables other than frequencies the formula may be modified as,

$$\chi^2 = \sum_{i=1}^{N} \frac{(exp_i - obs_i)^2}{\sigma_i^2} \tag{2.15}$$

where σ_i denotes the standard deviation in ith observed value. $\chi^2 = 0$ means a perfect agreement between the observed and expected values. The no. of degrees of freedom (dof) is determined by the no. of data points, the no. of parameters involved in the expected distribution (function), and any other condition imposed on the data. The χ^2/dof value is used to estimate the goodness of a fit at a particular level of confidence.

2.2.2 Geometric Measurements in Emulsion

All the geometric measurements should be made with a full knowledge of the distortion effects of emulsion. The geometric measurements consist of determining the coordinates of points in a suitable coordinate system, measurement of distances between two points, measurement of area and volume, measurement of projected and space angles, measurement of deviation of a track from a straight line, measurement of angular (spatial) distributions etc. For geometric measurements, it is essential that the eyepiece graticule has engraved on it a scale that divides the useful field diameter into equal parts (say 100). The useful field diameter is perhaps $50 - 70\%$ of the extreme field diameter. At a magnification of 1000, one division of the graticule usually is in order of magnitude of 1μm. The coordinates of a point in the field can then be measured with a standard deviation of less than a micron. One can at first choose an arbitrary point as the origin of the coordinate system that can easily be relocated later. For example in case of an interaction, the point of interaction can serve the purpose. One can then easily measure the x and y coordinates of any point in the horizontal plane with respect to the origin. The z coordinate is determined by the vertical displacement of the stage (and hence the emulsion plate) between the positions of two points having same x and y coordinates. This displacement of course

must be corrected by the emulsion shrinkage factor as has been mentioned earler.

The angle of dip (δ) of a linear track segment is given by $\tan\delta = S\,\Delta z/L_{xy}$, where Δz is the measured vertical difference between two points on the track segment under consideration, and L_{xy} is the length of the track projected between these two points on the horizontal $(x-y)$ plane. It has been implicitly assumed that the refractive index of the oil commonly employed for oil immersion objectives is very close to the refractive index of the developed emulsion and the glass plate. For dry objectives the real depth should be corrected by the refractive index of the with respect to that of the emulsion. The space angle also called the emission angle (θ), between two tracks may also be measured by the simple coordinate method. If two tracks are characterized by direction cosines (l_1, m_1, n_1) and (l_2, m_2, n_2), respectively, then θ is given by,

$$\cos\theta = l_1 l_2 + m_1 m_2 + n_1 n_2. \tag{2.16}$$

If all three coordinates of any two points on a track are given by (x_1, y_1, z_1) and (x_2, y_2, z_2), the direction cosines are obtained as,

$$l = \frac{(x_1 - x_2)}{[(x_1 - x_2)^2 + (y_1 - y_2)^2 + (z_1 - z_2)^2]^{1/2}},$$

$$m = \frac{(y_1 - y_2)}{[(x_1 - x_2)^2 + (y_1 - y_2)^2 + (z_1 - z_2)^2]^{1/2}},$$

$$n = \frac{(z_1 - z_2)}{[(x_1 - x_2)^2 + (y_1 - y_2)^2 + (z_1 - z_2)^2]^{1/2}}.$$

Thus in order to find out the emission angle of any secondary track coming out of an interaction, it is necessary to find out the direction cosines of the incident projectile track as well as those of the secondary track. The azimuthal plane is defined as a plane perpendicular to the direction of motion of the projectile nucleus. The track direction projected in this plane with respect to some reference direction may be defined as the azimuthal angle (φ) of a track (measured counterclockwise). If the projectile direction is absolutely coinciding with one of the horizontal displacement directions of the stage (say x-direction), then

$$\varphi = \tan^{-1}\left(\frac{\Delta z}{\Delta y}\right).$$

If the projectile direction is not completely coinciding with the x-direction of the stage motion, then φ for a particular track may be measured by setting the corresponding quantity for the projectile track to be equal to zero.

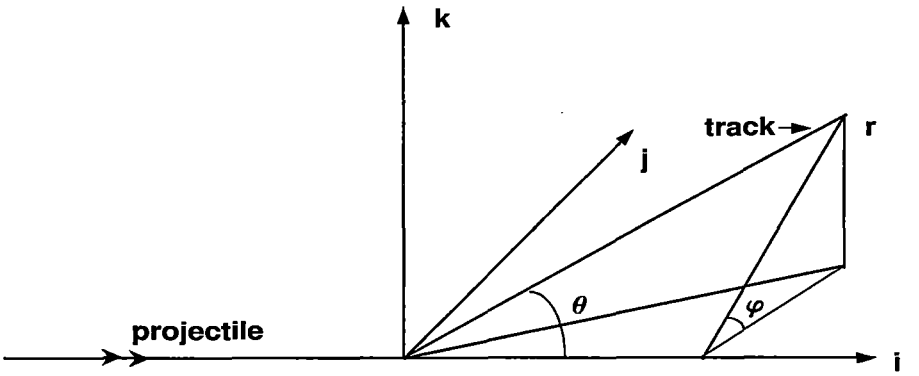

Figure 2.1: Schematic description of secondary track geometry with respect to a primary projectile track.

The track geometry has been schematically represented in Fig. 2.1. Due to scattering the track of a charged particle may not always be straight. Therefore, it is convenient to break up the track into M number of essentially straight segments, and the residual range of the particle may be determined from the relation,

$$R = \sum_{i=1}^{M} [(x_i - x_{i-1})^2 + (y_i - y_{i-1})^2 + S^2 (z_i - z_{i-1})^2]^{1/2},$$

where S is the shrinkage factor along the vertical (here z) direction. For mounted plates generally no shrinkage factor is associated along either of the horizontal directions.

In high energy heavy-ion interactions the number of secondary particles per event is very large. Therefore, in order to get sufficient spatial separation between two adjacent tracks, it may be necessary to displace the stage to such a large distance, that the point of interaction is far beyond the field of view containing the interaction vertex. There is every chance that the particle under consideration will suffer from Coulomb scattering and will deviate from its original direction. The problem is more acute in the forward direction, that is densely populated by jets of particles. Under such situations one may have to take help of a nearby projectile track located within the same field of view, that is essentially moving parallel to the projectile track under consideration. It is to be noted that if the projectile tracks are close to each other, they will experience almost identical distortions in the emulsion. Heavy-ion interactions are rich sources of highly energetic photons. These photons may interact with the nuclear field available in the emulsion

medium itself and produce e^-e^+ pairs. The angular separations between the electron and positron tracks are often very small and it is therefore, often extremely difficult to identify them as two separate tracks. Moreover, if the $\gamma \rightarrow e^-e^+$ conversion takes place near the interaction vertex, then it is also very likely to confuse the e^-e^+ tracks as originating from the interaction vertex. When the coordinates of points are recorded at a large distance from a particular interaction vertex, there may be interference with the tracks coming from other interaction points. These problems can be solved by recording the coordinates of several points on a single track, and through a reconstruction program obtain the best fitted straight line for them, and also to check whether or not that straight line is passing through the coordinates of the interaction vertex.

Momentum Measurement: A charged particle moving through matter experiences frequent small deflections due to elastic scattering with the Coulomb field offered by the atomic nuclei present in the medium. The probability for a particular deflection is given by Rutherford's scattering formula - small angular deviations occur with high frequency. The distribution follows a Gaussian pattern with the mean at zero. The theoretical treatment suitable for comparison with experiment suggests the mean absolute angular deflection $< \phi >$ to be measured. For convenience of measurement ϕ is considered as the projected angle on a plane of the space angle, and its mean value is given by [19],

$$< \phi >= \sqrt{\bar{\phi}^2} = \frac{2\,z\,e^2\,(Z^2Nd)^{1/2}}{p.\beta}\left[\ln\left(\frac{\phi_{max}}{\phi_{min}}\right)\right]^{1/2}, \tag{2.17}$$

where N = number of atoms per unit volume in emulsion, z = atomic number of the particle, p = momentum of the particle in MeV/c, β = velocity of the particle in the unit of c while traversing a path length = d, Z = the average atomic number of the atoms present in the medium, and ϕ_{max} (ϕ_{min}) = the maximum (minimum) value of the projected angle in the plane of the initial particle trajectory. Following a method suggested by Fowler [20], the mean absolute scattering angle $< \phi >$ can be determined. In this method the plate is placed on the mechanical stage of the microscope in such a way that the track is approximately parallel to the abscissa of the stage, say x-axis. The co-ordinates (x_0, y_0) of an arbitrary point on the track are measured. The plate is then displaced by a distance equal to the cell length d along x-direction, and the ordinate y_1 of the point is determined by means of an eyepiece scale. The measurement should be performed under high magnification (e.g., 2500×), and the ordinary eyepiece scale is

commonly replaced by a flair micrometer, which is capable of reading distances within a few hundreds of micron. Once again the stage is moved through the standard distance d, and the ordinate y_2 is recorded. The operation is repeated several times along the length of the track. The absolute value of the second differences taken irrespective of the sign $D_k = |y_{k+2} - 2y_{k+1} + y_k|$ of successive such measurements are determined. The mean absolute value between successive chords of length d corrected for stage noise and cell length $< D >= \sum_k^n D_k/n$ gives a measure of the scattering parameter,

$$< \phi >= \frac{< D >}{d} (180/\pi) \tag{2.18}$$

from which $p.\beta/z$ in MeV/c can be evaluated. If $< \phi >$ is to be a meaningful quantity, then in a given cell length d of the track, the energy loss is considered negligible.

2.2.3 Scanning in Emulsion

In a scanning program events of certain types are sought in a systematic way. Area (more specifically volume) scanning of a plate is usually done in strips approximately equal in width to a side of an inscribed square within the field of view. During the process the focal surface is continually shifted to sweep up and down from the surface of the emulsion to that of the glass by rotating the fine focus control, while observing events successively coming into and going out of the view. One such elementary motion down or up can be termed as scanning traverse. For high efficiency the field may be divided into a number of sufficiently small separate areas, so that the entire volume can be covered as the traverse is made. The field is not shifted until a particular volume has been completely searched. Generally area scanning is performed under either of the following two circumstances, (i) when events of a certain type within a given volume of emulsion are to be found, and (ii) if the situation demands a representative sample of events. Preliminary volume scanning may be performed under a total magnification of $300 - 400\times$ ($15\times$ ocular and $20\times$ dry objective, or $10\times$ ocular and $40\times$ oil immersion objective). The collected data can be finally refined under $1500\times$ total magnification ($15\times$ ocular and $100\times$ oil immersion objective). As high multiplicity events easily catch human eyes, with volume scanning it's seldom possible to get an unbiased sample of events. For that purpose the technique of along the track scanning is preferred. In this technique each

projectile track is carefully followed from the leading edge of a plate along its length until the projectile interacts or leaves the plate. Just like in the case of volume scanning, in this case too preliminary scanning may be performed under $300 - 400\times$ total magnification, but the final selection of events has to be done under $1500\times$ total magnification. It is a tiresome and time consuming process, and it requires a lot of concentration on the part of a scanner, and accuracy of experimental results depends largely on the experience and skill of the observer. To avoid individual bias counter checking of the same data sample by independent observers is recommended. Through along the track scanning it is possible to acquire a sample of events with minimum bias.

2.3 Advantages and Disadvantages of Emulsion Technique

One of the main advantages of nuclear emulsion is that it serves as a detector of charged particles as well as it provides different targets like H, C, O, N, Ag, and Br nuclei of varying mass numbers. As far as high energy interactions are concerned, information regarding target nucleus mass (size) dependence can therefore be obtained. Nuclear emulsion has the capacity to detect all charged particles coming out of an interaction. Thus nuclear emulsion is one of the very few detectors that have 4π acceptance. However, the detection efficiency may not be equally good in all directions. Particularly the efficiency is not very good along the vertical (along the thickness of the plate) direction. Due to a high medium density, the stopping power and therefore, the probability of interaction between a projectile particle and a target nucleus is high in case of nuclear emulsion. As a detector nuclear emulsion is less costly, light and can be handled very easily. The nuclear emulsion is also a very useful detector in cosmic ray experiments. As it can register all the charged particles with energy from very low up to the relativistic limit, and because the sensitivity of nuclear emulsion lasts for a few weeks, all charged particles within a sufficiently long time span can therefore be recorded. Therefore, it is suitable for balloon flight and satellite experiments. Nuclear emulsion permanently registers the trajectory of charged particles and tracks belonging to different types of particles have their own characteristic appearances. Hence if need arises, they can be distinguished from one another with a

little extra effort. In nuclear emulsion neutral particles can also be indirectly identified, as and when they interact with the nuclei present within the medium and produce tracks of charged particles. Nuclear emulsion has a large operating range with respect to temperature - from the temperature of liquid helium up to the boiling point of water. The most striking advantage of nuclear emulsion is its high spatial resolution. For conventional horizontally irradiated stacks of emulsion plates (or pellicles), in spite of multiple Coulomb scattering and distortion effects an accuracy of 0.1 unit of pseudorapidity can be achieved. If distributions of produced particles are to be analyzed in narrow intervals of pseudorapidity space, this unique feature makes the emulsion as competitive a detector as its large and much more costly electronic counterparts.

The nuclear emulsion has also quite a few limitations. One can not distinguish between the sign of a charge unless a magnetic field is applied. But it is difficult to get the magnetic field penetrate into the emulsion material, hence to produce enough curvature in the track of a relativistic particle to identify its charge. The tracks formed in emulsion are relatively small and hence they can be studied only under a microscope with high magnification. This makes the data acquisition process a tedious and time consuming one. For AB interactions where a few hundreds of particles are produced per event, the time taken to build up a statistics of an acceptable size is typically of the order of a few years. Moreover, till date human eyes remain most suitable for tasks like counting and identification of events and tracks. Therefore, the collected data can never be fully free from personal bias and errors. However, such limitations can be reduced through counter checking by more than one independent observers. Measurement of energy, momentum and mass of a particle in emulsion is so cumbersome and time consuming that such a proposition is often considered as impractical, and for routine investigations they are almost never undertaken. The sensitivity and the thickness of emulsion pellicles are affected by factors like temperature, humidity, age etc.. Unless proper care is taken in this regard, such factors induce extra errors in measured values. Because the identification of target fragments is often extremely difficult, and sometimes even impossible, therefore, in this technique its often impossible to exactly identify the target nucleus of an interaction. However, as later mentioned, there are ways by which one can make a gross distinction between the light group (H,C,N,O) and heavy group (Ag,Br) of target nuclei.

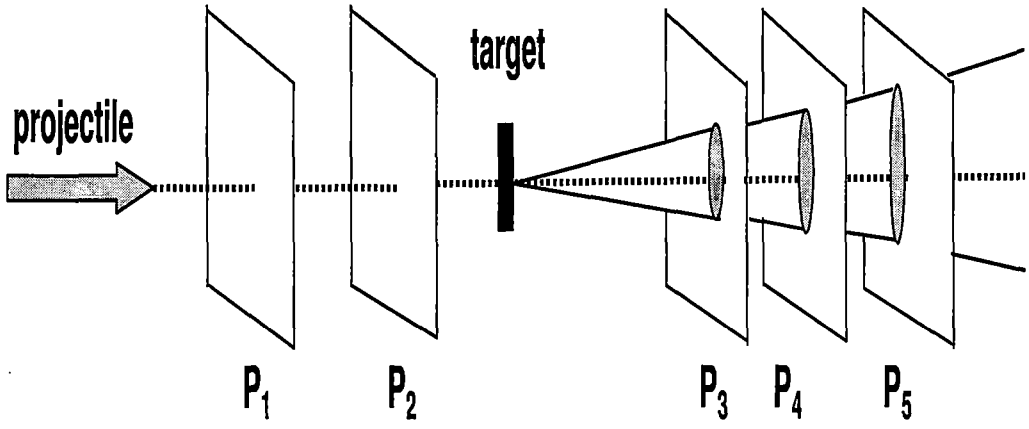

Figure 2.2: Schematic description of an emulsion chamber set up. P_1, P_2 P_3 etc. represent the emulsion coated plastic plates.

In the recent past in stead of standard stacks of emulsion pellicles, the emulsion chamber arrangement has been used in several emulsion experiments [21]. In this technique, thin plastic (acrylic or polystyrene) plates of typical dimension $10 \times 10 \times 0.1$ cm^3, coated on both side with emulsion layers are used. The thickness of emulsion coating is of the order of $2-3 \times 10^2$ μm. These emulsion plates are separated by honeycomb paper spacers with a few $2-3 \times 10^2$ μm thick metal targets (e.g, Pb or Au) placed in between. The incident beam travels perpendicularly through the arrangement, mostly through empty space. As the tracks travel mostly through empty space they suffer much less multiple Coulomb scattering. The position coordinates of the tracks are measured in the emulsion-air and emulsion-plastic interfaces with respect to other primary beam tracks. This substantially reduces the distortion effect. Thus in the chamber technique an accuracy of 0.01 pseudo-rapidity unit can be achieved. Because of the novel design of the emulsion chamber, it is possible to separate out all the tracks coming from an interaction, as they can be followed over as large a distance as several centimeters. However, there are a few disadvantages of this technique as well. Only area scanning (to be explained later) is possible in this technique, and an event sample with minimum bias can not be obtained. Another disadvantage is that the particles moving in the backward direction can not be traced, thereby limiting the pseudorapidity acceptance of the system. However, the central particle producing region can still be covered.

2.4 General Characteristics of the Data

In an emulsion experiment (Expt. no. EMU08) performed by the Buffalo group, Ilford G5 type nuclear photographic emulsion pellicles were horizontally exposed to a beam of ^{32}S nuclei at an incident momentum of 200A GeV/c obtained from the Super Proton Synchrotron (SPS) at CERN, Geneva [22]. The ^{32}S beam flux was 10^3 particles per square centimeter, and as mentioned before, the dimension of the emulsion plates at the time of exposure was $18 \times 7.5 \times 0.06$ cm^3. The emulsion plates were scanned along the track with the help of Leitz Metalloplan microscopes under a total magnification of 300× by two independent observers, so that the bias in event detection can be minimized. Periplan eyepieces (10×, 15×) in conjunction with (10×, 0.30) dry, (20×, 0.50) dry, (40×, 0.70) oil immersion, and (100×, 1.32) oil immersion objectives were used. Figures within each bracket denote respectively, the magnification and the $N.A.$ of the lens system. The accuracy of coordinate measurement was 1μm along the horizontal $(x - y)$ directions and 0.5μm along the vertical (z) direction. If an interaction has occurred within 20μm of either the top (emulsion-air) or bottom (emulsion-glass) surface, it has not been taken into account. Angle measurement of tracks becomes difficult for such events located near the interface of two different medium. Due to the same reason events occurring within 4 mm of the leading edge of the plate have also been excluded, as such regions are often plagued by severe distortion. A total path length of 127.38 mt was followed, within which a total number of 1354 inelastic ^{32}S-emulsion interactions were found. This resulted in an interaction mean free path $\lambda = 9.41 \pm 0.26$ cm, that is related to the total cross-section through $\sigma_{S-Em} = 1/N\lambda$, and the value is $\sigma_{S-Em} = 1150 \pm 34$ mb. Recall that the no. of scattering centers (N) present in emulsion is 7.898×10^{22} per cc (Table 2.2). After finding out a primary interaction induced by the incoming ^{32}S projectile, the number of secondary tracks in an event belonging to each category was counted. According to the emulsion terminology, tracks coming out of an interaction can be classified into four categories namely, the shower tracks, the gray tracks, the black tracks and the projectile fragments.

1. The shower tracks are created by singly charged particles moving at relativistic speed ($\beta \approx 0.7$). This category mainly comprises of particles produced in a high-energy interaction, most of which are charged π mesons. The total number of shower tracks in an event

is denoted by n_s. The ionization of shower tracks $I \leq 1.4\, I_0$ where I_0 is the minimum ionization in emulsion. For the Ilford G5 type of plates used in the present investigation this value is $I_0 = 20$ grains per 100μm.

2. The gray tracks are generally due to the protons that have directly participated in an interaction, and are knocked out from the target nuclei. They usually fall within an energy range of $30 - 400$ MeV. The ionization of these tracks is $1.4I_0 < I \leq 6.8I_0$. The range of a gray track is > 3 mm in emulsion, and the particle velocity is within $0.3c - 0.7c$. A few percent of the gray tracks may also be due to the slow moving mesons. The number of gray tracks in an event is denoted by n_g.

3. Black tracks are due to the slow moving heavy target fragments emitted by the remaining part of the excited target nucleus after an interaction has taken place. The process is similar to the evaporation of a heated liquid drop. These tracks have ionization $I > 6.8I_0$, range less than 3 mm in emulsion, and for a black track caused by a proton the velocity $< 0.3c$. The corresponding kinetic energy is less than 30 MeV. The number of black tracks in an event is denoted by n_b.

4. The projectile fragments are the spectator parts of the incoming projectile nucleus. They remain confined within an extremely narrow forward cone of small semi-vertex angle (θ_f), that depends on the momentum of the incoming nucleus. The tracks are very straight as they suffer very small Coulomb scattering. According to a simple Fermi gas model of a nucleus, the Fermi energy of a nucleon is given by,

$$E_f = \frac{\hbar^2}{2m_p}\left(\frac{3}{2}\pi^2 n_p\right)^{2/3},$$

where m_p and n_p are, respectively, the nucleon mass and nucleon number density. Numerically E_f is estmated as 21 MeV, and the corresponding Fermi momentum $p_f \approx 200$ MeV/c. For a nucleus having 200A GeV/c incident momentum, $\theta_f = 1$ mrad. In an event n_{pf} denotes the number of projectile fragments of charge $z \geq 2$ falling within this cone.

The sample of inelastic interactions can be classified into two different categories namely, the electromagnetic dissociation (ED) events and the nuclear events. Extremely strong electromagnetic fields offered by the target nuclei causes ED of the projectile nuclei. The impact parameter (b) for such an interaction $\geq$ sum of radii of the target and projectile. Such events typically consist only of projectile fragments [23]. Barring the ED events, rest of the events in the sample may be considered as nuclear interactions. After eliminat-

ing the ED events as well as the ^{32}S-H interactions, the mean free path for other nuclear interactions came out as $\lambda_{nucl} = 11.01 \pm 0.32$ cm. The no. of H-atoms present in emulsion is 3.2156×10^{22} per cc. If this no. is subtracted from the total no. of scattering centers per cc. then the cross-section comes out as, $\sigma_{nucl} = 1940 \pm 57$ mb. From simple geometric considerations of a participant spectator model [24] the nuclear cross-section is given by,

$$\sigma_{nucl}^{th} = \pi r_0^2 \left[A^{1/3} + B^{1/3} - \delta\right]^2. \tag{2.19}$$

With projectile mass no. $B = 32$, and excluding the contribution from H-nuclei the weighted average target mass no. of emulsion $A = 48.39$. This gives us $\sigma_{nucl}^{th} = 1904.3$ mb., where $\delta = 0.83$ and $r_0 = 1.3$ fm. have been used.

The nuclear interactions can also be subdivided into peripheral (large b) and central (small b) collisions by looking at their respective shower multiplicities. The number of heavy tracks in an event (n_h) is given by, $n_h = n_b + n_g$. By putting a condition on the number of these heavy target fragments like, $n_h \geq 8$ with at least one fragment of $Z \geq 2$ per event, it can be ensured that a subsample consisting only of ^{32}S-Ag/Br interactions are taken into account. The events with $n_h < 8$ can either be an Ag/Br, or a H/C/N/O interaction. A further restriction on the number of spectator projectile fragments in an event $n_{pf}\,(z \geq 2) = 0$, enabled us to choose only those interactions for which total fragmentation of the incident ^{32}S nuclei have taken place. Assuming each ^{32}S-Ag/Br interaction as an entirely incoherent set of 32 independent NN collisions, the total center of mass (cm) energy $\sqrt{s} \approx 620$ GeV. On the other hand, if the ^{32}S nucleus interacts as a single coherent object (see section 1.3.4) with an Ag ($A = 108$) or a Br ($A = 80$) nucleus, then the corresponding center of mass energy will, respectively be $\sqrt{s} \approx 1145$ GeV or $\sqrt{s} \approx 984$ GeV. The actual center of mass energy is perhaps somewhere in between the two extreme cases mentioned above, because (i) neither all interactions between two nuclei are coherent, and (ii) nor in a mixed sample of central and semicentral interactions, where the impact parameter does not have a fixed value, all nucleons belonging to the target and projectile nuclei always directly participate in the interactions. However, the purpose of quoting the above values of $\sqrt{s}$ is only to give an idea about the (cm) energy scale at which particle production is taking place, and not to determine the exact degree of coherence.

After counting measurements are completed, the emission angle (θ) and the azimuthal

angle (φ) of each track with respect to the incident projectile track were measured. This has been done by using 100× oil immersion objectives and at a total magnification of 1500×. As mentioned in section 1.2, the rapidity variable previously defined as,

$$y = \frac{1}{2}\ln\frac{E + p_l}{E - p_l}, \tag{2.20}$$

additive under Lorentz boost, can be used to locate a particle in a one dimensional phase space. Here E and p_l are, respectively, the energy and longitudinal component of linear momentum of the particle. The pseudorapidity variable,

$$\eta = -\ln\tan\frac{\theta}{2}, \tag{2.21}$$

is a convenient replacement of the rapidity variable, where energy and/or momentum measurements are difficult as it is the case for emulsion experiments, and where in comparison with the total energy the rest energy of a particle can be neglected, as it is the case for most of the charged mesons produced in high-energy interactions. The resolution in η as a function of θ is given by,

$$\delta\eta = -\frac{1}{\sin\theta}\delta\theta.$$

So, at small angles only a small error in θ can ensure a good resolution in η. Together with the azimuthal angle (φ), the pseudorapidity (η) variable constitutes a two-dimensional phase space. Distribution of both η and φ for all shower tracks in our event sample have been obtained in terms of the respective density functions namely, $\rho(\eta) = N_{ev}^{-1}(dn_s/d\eta)$ and $\rho(\varphi) = N_{ev}^{-1}(dn_s/d\varphi)$. $N_{ev} = 200$ is the total number of events in the sample. The η-distribution has been fitted with a Gaussian function like,

$$\rho(\eta)d\eta = \rho_0 \exp\left[-\frac{(\eta - \eta_0)^2}{2\sigma_\eta^2}\right] d\eta, \tag{2.22}$$

where ρ_0 is the peak density, η_0 is the peak position and σ_η is the standard deviation of the Gaussian distribution. The experimental histogram and the fitted Gaussian curve are both plotted in Fig. 2.3(a). One can see that, the Gaussian function well describes the η-distribution. Values of the fit parameters of the Gaussian curve along with average no. of each category of tracks in the event sample are given in Table 2.5. One similar plot for the φ-distribution can be seen in Fig. 2.3(b). Within statistical uncertainties $\rho(\varphi)$ is found to be uniformly distributed in between $\varphi = 0 - 360$ degree. The dips near $\varphi = 90^0$

and 270^0 are to be noted. Most probably they are due to inefficient recording of shower tracks in directions vertical to the emulsions plates, and exactly toward or away from the direction of vision.

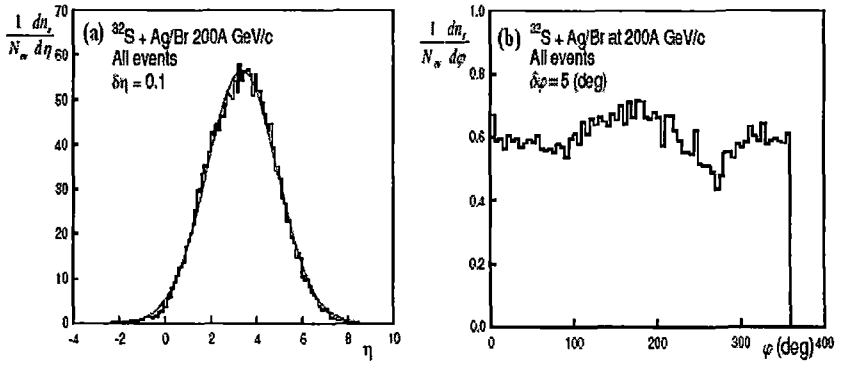

Figure 2.3: (a) Pseudorapidity η and (b) azimuthal angle φ distribution of shower tracks emanating from ^{32}S-Ag/Br interactions at 200A GeV/c.

The no. density of shower tracks in the central pseudorapidity region is a good measure of the centrality of the collision. Following a method suggested by Wong [25], an estimate of the average impact parameter ($\bar{b}$) for the sample of events used in the analysis can be obtained. In this method the peak value of the pseudorapidity density of produced charged particles in AB collision at an impact parameter b, and at a particular incident momentum per nucleon, is related to the same density for pp interaction at the same momentum by the following formula,

$$\frac{dn_{AB}}{d\eta}(b)\Big|_{peak} \approx 1.28\,\frac{AB}{A^{2/3}+B^{2/3}}\,\frac{1}{1+a(A^{1/3}+B^{1/3})}\,\exp(-b^2/2\beta^2)\,\frac{dn_{pp}}{d\eta}\Big|_{peak}. \quad (2.23)$$

In pp interaction at laboratory momentum 200 GeV/c ($\sqrt{s}$ = 19.4 GeV), the peak density of particles = 1.38 [26]. A and B are the mass no. of the interacting nuclei, and a (= 0.09) is a parameter obtained by linearly fitting $dn_{ch}/d\eta$ against $B^{1/3}$ for different AB collisions at 200A GeV/c [25]. In our case B = 32, whereas the weighted average mass no. of target Ag or Br nuclei $A \approx 94$. Putting these values in Eq. (2.23) one can determine the factor $\exp(-b^2/2\beta^2)$. In the above formula, $\beta^2 = {\beta_A}^2 + {\beta_B}^2 + {\beta_p}^2$, $\beta_A = r_0 A^{1/3}/\sqrt{3}$, $\beta_B = r_0 B^{1/3}/\sqrt{3}$, $r_0 (= 1.05fm)$ is the radius parameter and $\beta_p (= 0.68fm)$ is a

thickness parameter for NN collision. Substituting these values in Eq. (2.23) an estimated average value of the impact parameter ($\bar{b}$) for a sample of events can be obtained. The impact parameter values for our sample and subsample of events are quoted in Table 2.5. It should be noted that in obtaining $\bar{b}$ the rapidity distribution is replaced by the η distribution. However, at high energies they do not differ significantly from each other. The value of impact parameter obtained in this manner may not be treated as an exact one. It only gives us a rough idea about the average centrality of the event sample used. While investigating issues like dynamical fluctuation, it is imperative to restrict all other trivial sources of fluctuation originating from widely varying collision geometry or widely fluctuating no. of particles from one η bin to the other. The contribution from fluctuating geometry is marginal to our results, because a high value of average shower multiplicity and total fragmentation of the incident projectile in all events substantially restrict the range of b. The geometry dependence of the colliding system can be better understood if the sample is partitioned based on shower multiplicities. Three subsamples, almost equal in size, have been obtained in this way with the criteria, $n_s < 175$, $175 \leq n_s \leq 275$ and $n_s > 275$. For each subsample the average multiplicity of each category of tracks has been determined and quoted in Table 2.5. The η distribution for each subsample has also been obtained and fitted with the respective Gaussian functions. The fit results are also presented in Table 2.5. With increasing $< n_s >$, a shift in η_0 towards lower value is to be noted. This probably is an outcome of more stopping of the projectiles by the target nuclei with increasing centrality. The $\bar{b}$ values are also computed for each set of data, and included in the same Table. As expected, there is a mark decrease in $\bar{b}$ value with increasing $< n_s >$. The energy density in the central η region can now be estimated keeping two points in mind: (i) the sample with $n_s > 275$ has the highest centrality, and one may assume that the overlapping area ($\mathcal{A}$) between ^{32}S projectile and Ag/Br target is almost equal to the geometrical area of a ^{32}S nucleus; (ii) one has also to remember that the production of neutral π mesons in any high energy interaction is as abundant as either of their charged varieties. Therefore, while using Bjorken's formula $N_{ev}^{-1}\,(dn_s/d\eta)$ has to be replaced by,

$$N_{ev}^{-1}\,(dn_{all}/d\eta) \;=\; 1.5\,N_{ev}^{-1}(\,dn_s/d\eta). \tag{2.24}$$

Keeping these two factors in mind and putting $< m_t >= \sqrt{m^2 + < p_t >^2} \approx 0.38$ GeV, and the proper formation time $\tau_0 = 1$ fm/c into,

$$\epsilon = \frac{< m_t >}{\tau_0 \mathcal{A}} \left. \frac{dn_{all}}{d\eta} \right|_{\eta=\eta_0}, \tag{2.25}$$

one gets, $\epsilon \approx 1.3$ GeV/fm^3. Note that even for the subsample with highest no. of produced particles, the value is equal to just about the threshold required for the onset of a QGP like state, which according to the lattice QCD calculations is $\sim$ a few GeV/fm^3 [27].

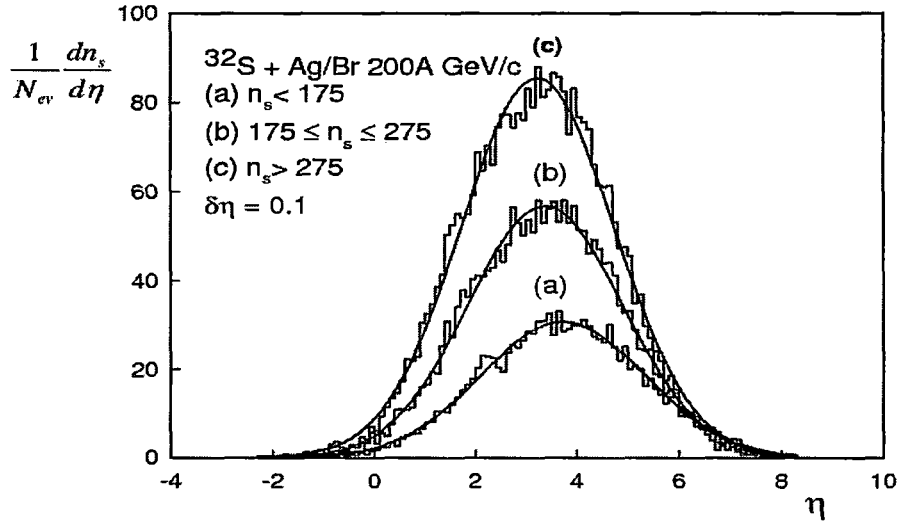

Figure 2.4: Pseudorapidity η distribution of shower tracks when the entire event sample has been divided into three subsamples.

As mentioned earlier, the experimental results have also been compared with those obtained by analyzing events generated with the computer code FRITIOF based on Lund Monte Carlo model [28] for high energy AB interactions. The model assumes that, as two nucleons collide with each other particle production takes place through the creation of longitudinally excited strings between the constituents of the same nucleon. The strings subsequently fragment, and new hadrons originate. An AB collision is considered to be a combination of multiple collisions between the nucleons belonging to one nucleus with those of the other. A large sample (7×10^4) of ^{32}S-emulsion events has been generated

using the Lund Monte Carlo Code FRITIOF, where the proportional abundance of different categories of target nuclei present in the emulsion material (Table 2.2) has been taken into account.

Table 2.5 Gross features of the ^{32}S-Ag/Br data sample. Standard errors are quoted within first brackets.

Event sample	No. of events	$< n_s >$	$< n_g >$	$< n_b >$	η_0	ρ_0	σ_η	$\bar{b}$ fm
All	200	217.79 (6.16)	4.66 (0.23)	8.99 (0.35)	3.37 (0.008)	56.34 (0.26)	1.55 (0.008)	3.77
$n_s < 175$	71	123.24 (3.83)	2.75 (0.35)	6.31 (0.68)	3.72 (0.01)	30.69 (0.21)	1.62 (0.01)	5.34
$175 \leq n_s \leq 275$	65	215.35 (3.77)	6.02 (0.97)	11.82 (0.96)	3.37 (0.01)	56.71 (0.34)	1.53 (0.01)	3.75
$n_s > 275$	64	319.94 (3.88)	6.31 (0.36)	9.92 (0.48)	3.23 (0.01)	85.44 (0.52)	1.51 (0.01)	2.10

From the generated sample a ^{32}S-Ag/Br subsample has been so filtered out that it has the same multiplicity distribution of produced particles as the corresponding shower track multiplicity distribution of the experimental data set. The size of generated event sample is ten times as large as the experimental one. Event samples have also been simulated by generating (pseudo) random numbers. In this case the phase space variables associated with each shower track (η, φ) have been replaced by a pair random numbers. The sample size is once again ten times the size of the experimental one, and the shower multiplicity distribution is same as the experimental one. While generating the random numbers, independent emission of particles has been assumed with no correlation whatsoever between these particles being produced.

Bibliography

[1] M. Reingamum, *Z. Physik.* **12,** 1076 (1911).

[2] A. Beiser, *Rev. Mod. Phys.* **24,** 273 (1952).

[3] C. F. Powell, P. H. Fowler, and D. H. Perkins, *The Study of Elementary Particles by Photographic Method* (Pergamon, Oxford), NY (1959).

[4] W. H. Barkas, *Nuclear Research Emulsions, Vol. I and II* (Academic Press, New York 1963).

[5] R. W. Gurney and N. F. Mott, *Proc. Roy. Soc. (London)* **A164,** 151 (1938).

[6] J. W. Mitchell, *Phil. Mag.* **40,** 249 (1949); *ibid,* **40,** 667 (1949).

[7] C. C. Dilworth, G. P. S. Occhiallini, and R. M. Payne, *Nature* **163,** 102 (1948).

[8] M. Blau and J. A. De Felice, *Phys. Rev.* **74,** 1198 (1948).

[9] Ilford Fact Sheet, http://www.illfordphoto.com (2005).

[10] M. S. Livingstone and H. A. Bethe, *Rev. Mod. Phys.* **9,** 245 (1937).

[11] M. Blau, *Phys. Rev.* **75,** 279 (1949)
M. Morand and L. van Rossum, *Fundamental Mechanisms of Photographic Sensitivity,* ed. J. W. Mitchell, (Butterworths Scientific Publications, London, 1951).

[12] C. O'Ceallaigh, *Nuov. Cim. Suppl.* **12,** 412 (1954).

[13] P. H. Fowler and D. H. Perkins, *Phil. Mag.* **46,** 587 (1955).

[14] M. A. Bloomer, H. H. Heckman, and Y. J. Karant, *Nucl. Instrum. Methods* **215,** 247 (1983).

[15] N. F. Mott, *Proc. Roy. Soc. (London)* **124,** 425 (1929)
B. Rossi, *High Energy Particles* (Prentice Hall, Englewood Chiffs, New Jersey, 1952).

[16] C. M. G. Lattes, G. P. S. Occhiallini and C. F. Powell, *Proc. Phys. Soc. (London)* **61,** 173 (1948).

[17] P. Freier, E. J. Lofgren, E. P. Ney, and F. Oppenheimer, *Phys. Rev.* **74,** 1818 (1948).

[18] M. R. Spiegel *Theory and Problems of Statistics*, (McGraw-Hill Book Co., UK, 1988).

[19] E. J. Williams, *Phys. Rev.* **58,** 292 (1940).

[20] P. H. Fowler, *Phil. Mag.* **41,** 169 (1950).

[21] I. Otterlund, *3rd Hellenic School on Elementary Particle Physics*, (Corfu, Greece, 1989)
S. Garpman *et al.*, *Nucl. Instrum. Methods* **A269,** 134 (1988).

[22] G. Singh, K. Sengupta and P. L. Jain, *Phys. Rev. Lett.* **61,** 1073 (1988)
P. L. Jain, K. Sengupta and G. Singh, *Phys. Rev.* **C 44,** 844 (1991).

[23] G. Singh, K. Sengupta and P. L. Jain, *Phys. Rev.* **41,** 999 (1990).

[24] G. D. Westfall *et al.*, *Phys. Rev.* **C19,** 1309 (1979).

[25] C. Wong, *Introduction to High-Energy Heavy-ion Collisions*, (World Scientific, Singapore, 1994).

[26] M.J. Tannenbaum, *Quark-Gluon Plasma* eds. B. Sinha, S. Paul and S. Raha, (Springer Verlag, Berlin, 1990).

[27] F. Karsch, *Proceedings of Quark Matter '01 Conference*, (Stony Brook, USA,2001), *Nucl. Phys.* **A 698,** 199c (2002).

[28] B. Andersson, G. Gustafsson, and B. Nilsson-Almqvist, *Nucl. Phys.* **B281,** 289 (1987)
B. Nilsson-Almqvist and E. Stenlund, *Comp. Phys. Commun.* **43,** 387 (1987).